NATIONAL ADVISORY COMMITTEE FOR AERONAUTICS

WARTIME REPORT

ORIGINALLY ISSUED
March 1940 as
Advance Confidential Report

ESTIMATION OF CRITICAL SPEEDS OF AIRFOILS AND STREAMLINE BODIES

By Russell G. Robinson and Ray H. Wright

Langley Memorial Aeronautical Laboratory
Langley Field, Va.

NACA

WASHINGTON

NATIONAL ADVISORY COMMITTEE FOR AERONAUTICS

ADVANCE CONFIDENTIAL REPORT

ESTIMATION OF CRITICAL SPEEDS OF AIRFOILS AND STREAMLINE BODIES

By Russell G. Robinson and Ray H. Wright

SUMMARY

Methods and charts are presented for estimating the critical compressibility speeds of a large number of airfoils and streamline bodies. A method introduced to allow for the combination of these parts permits the estimation of the critical speed of an airplane wing including the effects of fuselage and nacelles. The systematic effects of thickness, thickness distribution, camber, camber location, leading-edge radius, and lift coefficient are considered.

The results indicate that with a given lift coefficient the thickness of the airfoil or of the body is the primary factor controlling its critical speed. For high values of critical speed, the location of maximum thickness and maximum camber should be near the 50-percent-chord point. An airfoil should be designed to have a high value of the critical speed for the lift coefficient at which high-speed operation will occur.

INTRODUCTION

The critical speed is defined as the speed at which a breakdown in flow, caused by compressibility effects and known as the compressibility burble, occurs. This flow change is usually evidenced by a rapid rise in the drag coefficient. At about the same speed, there is generally a marked change in the lift coefficient. The difficulties of flight under such conditions are apparent. These adverse effects were first observed on propeller tips but, as the speed of flight is increased, the critical speeds of other parts of the airplane may be reached. It therefore becomes necessary to estimate whether the critical speed of any part of an airplane lies below the highest speed for which the airplane is designed and, if so, to choose an airfoil and body combination having a critical speed higher than the maximum speed of the airplane or at least having as high a critical speed as possible.

Because the propeller was the part of the airplane on which critical flow was first observed, investigation of the critical speeds of airfoils has been primarily concentrated on propeller sections. In addition to

the tests of propellers operating at high tip speeds, the results of tests of various airfoil sections suitable for use in propellers are available. Clark Y and R.A.F. 6 sections have been tested in the NACA 11-inch high-speed tunnel (reference 1). Among 16 related airfoils tested (reference 2), one suitable for propeller sections (the NACA 2409-34) was found to give lower profile drag at high speeds with low or moderate lift coefficients than propeller sections commonly used.

Experiments on an NACA 4412 airfoil reported in reference 3 were concerned with the investigation of the nature of the flow changes that occur in the high-speed range. The large increase in drag associated with the compressibility burble was shown to correspond to the loss of available energy behind a shock wave somewhat similar to that formed at the nose of a bullet in flight. The incipience of the shock wave was found to correspond rather closely to the attainment of the local speed of sound at some point on the airfoil. It was therefore concluded that critical speeds could be estimated with reasonable accuracy from a knowledge of the pressure or the velocity distribution.

The present report is concerned with the practical application of the method of predicting critical speeds from low-speed velocity distributions. The paper is divided into three sections. Part I briefly reviews the theoretical basis and discusses the accuracy and the limitations of the method used. The principal section, part II, presents and explains the use of charts for estimating critical speeds; this portion may be directly used for airplane design work without reference to the other sections. Part III discusses the shape characteristics indicated by the method to be desirable for high-speed airfoils.

This paper was originally prepared in 1939. Since that time further knowledge and additional understanding of compressibility effects have been obtained. Certain additions and revisions have therefore been made. The most important changes are (a) the substitution of the more accurate von Kármán compressibility factor for the factor $1/\sqrt{1 - M^2}$ previously used for estimating the change in pressure coefficient with Mach number, and (b) the inclusion of a method to allow for the necessary change with Mach number of the airplane lift coefficient.

I. THE USE OF PEAK PRESSURES IN ESTIMATING CRITICAL SPEEDS

This section briefly presents the theory and the experimental evidence for the occurrence of the compressibility burble and for the prediction of critical speeds for pressure or velocity distributions. The limitations of the method and the factors affecting its accuracy are also discussed.

Theory

As the speed of flight is increased, a speed – or more definitely a Mach number (the ratio of the speed of flight to the speed of sound in air) – is reached at which the local airspeed at some point on the airplane, for example on the wing, attains or slightly exceeds the speed of sound. Various considerations suggest that, at this speed, a shock wave may form, terminating the supersonic flow. (See reference 4.) The flow through the shock is nonisentropic and a loss in total pressure occurs. The corresponding increase in drag of the airfoil may be very large. The theory of shock waves and of compressible flow, both below and above the speed of sound, is discussed in reference 5.

The existence and the nature of shock waves on airfoils have been the subject of considerable investigation. Schlieren photographs have been obtained of shock waves on airfoils tested in the NACA 24-inch high-speed tunnel (references 3 and 6). Investigations have also been made of the drag increase, the change in lift, and the total pressure loss caused by these waves. Shock waves of somewhat less severity have been obtained on an airfoil tested in an open-throat tunnel in Italy (reference 7). Further study of the compressible flow is necessary to determine with quantitative accuracy the effect of compressibility on airplane performance. Nevertheless, experiment supports the conclusion that shock waves, involving large losses in efficiency, may occur on airfoils when the relative local velocity at any point reaches or slightly exceeds the speed of sound.

If the critical speed is assumed to be equivalent to the flight speed at which the speed of sound is attained at some point, the critical speed can evidently be predicted from a knowledge of the maximum velocity (or minimum pressure) on the airfoil. The required relation between peak negative pressure and critical speed will now be developed. The following symbols are used:

p	pressure
ρ	density
a	speed of sound $\left(\sqrt{\frac{\gamma p}{\rho}}\right)$
V	velocity
V_{cr}	critical velocity
γ	ratio of specific heats $\left(c_p/c_v\right)$ of air
q	dynamic pressure $\left(\frac{1}{2}\rho_o V_o^2\right)$
P	pressure coefficient $\left(\frac{p - p_o}{q}\right)$

M Mach number (V_o/a_o)

M_{cr} critical Mach number

t ordinary temperature, °F

T absolute temperature (460 + t), °F

Subscripts:

o values in the undisturbed stream

cr values when the local speed of sound has been reached at some point

i values for incompressible flow

From the Bernoulli equation for compressible flow,

$$\frac{p}{p_o} = \left(\frac{\rho}{\rho_o}\right)^{\gamma} = \left[1 - \frac{1}{2}(\gamma - 1)\frac{V_o^2}{a_o^2}\left(\frac{V^2}{V_o^2} - 1\right)\right]^{\frac{\gamma}{\gamma-1}} \qquad (1)$$

from which

$$\frac{a^2}{a_o^2} = \frac{\gamma p}{\rho}\frac{\rho_o}{\gamma p_o} = \frac{\rho_o}{\rho}\left(\frac{\rho}{\rho_o}\right)^{\gamma} = \left(\frac{\rho}{\rho_o}\right)^{\gamma-1}$$

$$= \left[1 - \frac{1}{2}(\gamma - 1)\frac{V_o^2}{a_o^2}\left(\frac{V^2}{V_o^2} - 1\right)\right] \qquad (2)$$

At the critical speed, the values of pressure, velocity, and speed of sound at the point where the local speed of sound has been attained are $p = p_{cr}$, $V = a_{cr}$, $a = a_{cr}$; so that, from equation (2),

$$\frac{a_{cr}^2}{a_o^2} = \left[1 - \frac{1}{2}(\gamma - 1)\frac{V_o^2}{a_o^2}\left(\frac{a_{cr}^2}{V_o^2} - 1\right)\right]$$

from which

$$\frac{a_{cr}^2}{a_o^2} = \frac{2}{\gamma + 1}\left(1 + \frac{\gamma - 1}{2}\frac{V_o^2}{a_o^2}\right) \qquad (3)$$

But

$$\frac{p_{cr}}{p_o} = \left(\frac{\rho_{cr}}{\rho_o}\right)^{\gamma} = \left(\frac{a_{cr}^2}{a_o^2}\right)^{\frac{\gamma}{\gamma-1}}$$

and thus

$$\frac{p_{cr}}{p_o} = \left[\frac{2}{\gamma+1}\left(1 + \frac{\gamma-1}{2}\frac{V_o^2}{a_o^2}\right)\right]^{\frac{\gamma}{\gamma-1}} \qquad (4)$$

$$a_o^2 = \frac{\gamma p_o}{\rho_o}$$

so that

$$p_o = \frac{\rho_o a_o^2}{\gamma}$$

and, from (4),

$$p_{cr} - p_o = \frac{\rho_o a_o^2}{\gamma}\left\{\left[\frac{2}{\gamma+1}\left(1 + \frac{\gamma-1}{2}\frac{V_o^2}{a_o^2}\right)\right]^{\frac{\gamma}{\gamma-1}} - 1\right\}$$

$$\frac{p_{cr} - p_o}{q} = \frac{2a_o^2}{\gamma V_o^2}\left\{\left[\frac{2}{\gamma+1}\left(1 + \frac{\gamma-1}{2}\frac{V_o^2}{a_o^2}\right)\right]^{\frac{\gamma}{\gamma-1}} - 1\right\} \qquad (5)$$

or, writing

$$\frac{V_o}{a_o} = M_o \qquad \gamma = 1.4 \text{ for air}$$

and letting

$$\frac{p_{cr} - p_o}{q} = P_{cr}$$

$$P_{cr} = \frac{1.43}{M_o^2}\left\{\left[0.834\left(1 + 0.2\,M_o^2\right)\right]^{3.5} - 1\right\} \qquad (6a)$$

or, if P is considered the independent variable,

$$P = \frac{1.43}{M_{cr}^2}\left\{\left[0.834\left(1 + 0.2\,M_{cr}^2\right)\right]^{3.5} - 1\right\} \tag{6b}$$

where M_{cr} is the critical Mach number. This equation gives the critical pressure coefficient P_{cr} corresponding to any Mach number M_o or the critical Mach number M_{cr} corresponding to any pressure coefficient P.

The critical speed V_{cr} corresponding to M_{cr} depends on the speed of sound

$$a_o = 49.1\sqrt{T_o} \text{ feet per second}$$
$$= 33.5\sqrt{T_o} \text{ miles per hour}$$

Therefore,

$$V_{cr} = \frac{V_{cr}}{a_o} \times a_o = M_{cr} \times 49.1\sqrt{T_o} \text{ feet per second}$$
$$= M_{cr} \times 33.5\sqrt{T_o} \text{ miles per hour}$$

Equation (6) cannot be used directly for the prediction of critical Mach numbers from low-speed or calculated pressure distributions because, in general, the absolute values of the pressure coefficient P increase with Mach number. Ackeret (reference 8) has shown that, for a particular form having small induced velocity, the pressure coefficient should theoretically increase (in absolute value) as $1/\sqrt{1 - M_o^2}$. He achieved this result by neglecting the two terms in the general equation of continuity that contain the velocity normal to the forward velocity as a factor. Both of these terms are small but one of them is not entirely negligible, even for a form only 1 percent thick. Glauert (reference 9) making the same assumption as to the thinness of the airfoil, obtained the same factor, $1/\sqrt{1 - M_o^2}$, for the increase in lift (or lift-curve slope); from these results it can be deduced that the average pressure coefficient should increase by this same factor. The increase with Mach number of lift-curve slopes for airfoils of moderate thickness is in approximate agreement with this theory. (See reference 5.) In most cases, even for moderately thick airfoils, the increase of the peak negative pressure coefficients follows approximately the factor $1/\sqrt{1 - M_o^2}$. (See, for instance, reference 3.) As the theoretical factor is applied to larger and larger values of the peak negative pressure coefficient $\left(-P_i\right)_{max}$, however, it is found increasingly to underestimate the rise in value with Mach number.

A factor given by von Kármán in reference 10, which takes account of this effect, is

$$\frac{1}{\sqrt{1 - M_o^2} + \frac{M_o^2 P_i}{2\left(1 + \sqrt{1 - M_o^2}\right)}}$$

When P_i is negative, this expression increases more rapidly with M than does $1/\sqrt{1 - M_o^2}$, and the larger the absolute value of P_i the more rapid is the increase. The von Kármán relation was derived by a study of the flow equation in the velocity plane (hodograph method). In order to obtain a general solution, the assumption $\gamma = -1$ was made. The derived factor thus strictly applies only to a fictitious gas for which $\gamma = -1$, but an approximate solution obtained by assuming $\frac{1 - M^2}{\rho^2}$ equal to a mean value $\frac{1 - M_o^2}{\rho_o^2}$ yielded an expression increasing with Mach number only a little more rapidly than that obtained by assuming $\gamma = -1$. The result obtained is clearly not greatly influenced by the value of γ used. Regardless of the theoretical questions involved, however, the expression

$$\frac{1}{\sqrt{1 - M_o^2} + \frac{M_o^2 P_i}{2\left(1 + \sqrt{1 - M_o^2}\right)}}$$

is shown by experimental evidence, of which that cited in reference 10 is only one example, to express the increase in absolute value of the negative pressure coefficient more accurately than $1/\sqrt{1 - M_o^2}$ and as accurately, in fact, as can be expected with any single mathematical formula.

Jacobs (reference 4), assuming that the pressure coefficients increase with Mach number according to the factor $1/\sqrt{1 - M_o^2}$, obtained a relation between the maximum low-speed negative pressure coefficient $(-P_i)_{max}$ and the critical Mach number. A similar relation can be obtained with the von Kármán factor by substituting

$$P \cong \frac{P_i}{\sqrt{1 - M_{cr}^2} + \frac{M_{cr}^2 P_i}{2\left(1 + \sqrt{1 - M_{cr}^2}\right)}}$$

in equation (6b), whence

$$P_i \cong \frac{P\sqrt{1 - M_{cr}^2}}{1 - \frac{M_{cr}^2 P}{2\left(1 + \sqrt{1 - M_{cr}^2}\right)}} \qquad (7)$$

where P is to be taken from equation (6b). Equation (7) forms the basis for the prediction of critical speeds from computed or low-speed pressure distributions. The critical Mach number M_{cr} of an airfoil is determined by the largest negative pressure coefficient $(-P_i)_{max}$ existing at any point on the surface.

Accuracy of the Method

The exactness with which critical speeds may be predicted from the critical-speed curve obtained from equation (7) depends on the correctness of the assumptions involved and also on the precision with which the pressure coefficients can be obtained.

The first assumption, that the compressibility burble corresponds to the attainment of the local speed of sound at some point on the airfoil, has been verified for two-dimensional flow by the results of reference 3. This assumption has also been verified in the case of three-dimensional flow over cowlings (reference 11).

Change of pressure with Mach number.- The second assumption, that the pressure coefficients increase in absolute value according to von Kármán's factor

$$\frac{1}{\sqrt{1 - M_o^2} + \frac{M_o^2 P_i}{2\left(1 + \sqrt{1 - M_o^2}\right)}}$$

may be compared with the results of Kaplan's theoretical investigations of the subsonic compressible flow about elliptic cylinders (reference 12) and about symmetrical Joukowski airfoils (reference 13). These investigations indicate that the peak negative pressures rise more rapidly than those at other points on the airfoil, a result which is in agreement with the theory of von Kármán. Experimental results on a Joukowski airfoil (reference 14), as well as unpublished pressure data obtained in the NACA 8-foot high-speed tunnel, show qualitative agreement with the theory of Kaplan. The rise of the peak negative pressures with Mach number, however, is more

rapid than that predicted by Kaplan's theory, which gives a rate of increase less than

$$\frac{1}{\sqrt{1 - M_o^2} + \frac{M_o^2 P_i}{2\left(1 + \sqrt{1 - M_o^2}\right)}}$$

This result may be due to insufficient accuracy of Kaplan's second approximation. Thus, the factor

$$\frac{1}{\sqrt{1 - M_o^2} + \frac{M_o^2 P_i}{2\left(1 + \sqrt{1 - M_o^2}\right)}}$$

seems to express the increase of the peak negative pressure coefficient more satisfactorily than the theory of Kaplan carried to a second approximation, although additional approximations may be expected to give better results.

Examination of a large number of pressure distributions obtained in the NACA 8-foot high-speed tunnel showed negative-pressure peaks increasing in some cases more rapidly and in other cases less rapidly than

$$\frac{1}{\sqrt{1 - M_o^2} + \frac{M_o^2 P_i}{2\left(1 + \sqrt{1 - M_o^2}\right)}}$$

For the cases in which von Kármán's factor underestimates the increase, figures 12(a), (b), (c) of reference 10 are typical in that the underestimation is usually small. In cases for which von Kármán's factor overestimates the increase, the difference may be large. The reasons for failure of the actual increase to follow the theoretical factor are now fairly well understood. The theory is based on the assumption that the flow follows the contour of the airfoil but actually, because of viscosity effects, the flow path often departs from the airfoil surface. This departure is always of such a nature as to tend to decrease the peak negative pressure coefficients. If at low speeds the flow in the vicinity of the position of the negative-pressure peak is laminar and fails to follow the airfoil contour, it may at higher speeds (larger Reynolds numbers) become turbulent and follow more closely the airfoil surface. The negative-pressure peaks may then increase more rapidly than by the factor

$$\frac{1}{\sqrt{1 - M_o^2} + \frac{M_o^2 P_i}{2\left(1 + \sqrt{1 - M_o^2}\right)}}$$

If, on the other hand, the flow is critical as regards separation throughout the Mach number range or if, because of Reynolds number or Mach number effects or a combination of both, it becomes critical, the tendency of the peak negative pressure coefficient to increase with Mach number may be counteracted by a wider departure of the flow from the contour, and the peak may fail to increase or may even decrease in value. Except for cases involving severe separation, which in itself produces effects similar to some of those observed when the critical speed is exceeded, the von Kármán factor generally expresses satisfactorily the experimentally determined increase of the peak negative pressure coefficients with Mach number.

The von Kármán factor was derived only for two-dimensional flow and generally overestimates the compressibility effect for three-dimensional flow. With bodies of revolution, for instance, the compressibility factor has been found theoretically to decrease with increasing slenderness of the body and to approach unity for fineness ratio approaching infinity. (See reference 15.) The critical speed of complete airplanes will not likely be determined by the pressures over slender bodies, however, because the velocities induced over such bodies are small; and for blunt bodies or other bodies having induced velocities comparable to those over wings the von Kármán factor may be assumed to apply with reasonable approximation. This assumption has been found to be correct for the very large peak negative pressure coefficients on radial-engine cowlings (reference 11) as well as for much lower peaks found on other bodies tested in the NACA 8-foot high-speed tunnel. In the case of the sphere, comparison with the theory of Kaplan (reference 16) indicates that the von Kármán factor may slightly overestimate the increase of peak negative pressure coefficient with Mach number. These examples suggest that for practical application the von Kármán factor

$$\frac{1}{\sqrt{1 - M_o^2} + \frac{M_o^2 P_i}{2\left(1 + \sqrt{1 - M_o^2}\right)}}$$

may satisfactorily estimate the increase in peak negative pressure coefficient for three-dimensional as well as for two-dimensional flows. The use of this factor in this report for three-dimensional flows is considered conservative.

Estimation of the peak negative pressure.- The pressure coefficients over the forward portions of airfoils and near the negative-pressure peaks can, in most cases, be computed with sufficient accuracy from the potential theory. But in the case of high, sharp, negative-pressure peaks, involving large positive pressure gradients, flow separation may occur, particularly at low Reynolds numbers; and the peak negative pressure coefficients can no longer be accurately computed. If separation occurs, the critical speed estimated from the computed peak may be too low because the predicted peak negative pressure is higher than that actually attained. On the other hand, critical speeds predicted from negative-pressure peaks obtained experimentally at low Reynolds numbers may be higher than the values actually attained at

higher Reynolds numbers because, as the Reynolds number is increased, peak negative pressures occurring near the nose tend to approach more nearly the theoretical value. The flow changes occurring near the critical speed are incompletely understood, but theoretical peak negative pressures may be a more satisfactory criterion for estimating the critical speeds than experimental values obtained at low Reynolds numbers.

High, sharp pressure peaks with the accompanying large positive pressure gradients causing separation usually occur near the leading edge. For a symmetrical airfoil, the height and the sharpness of the peak increase with the lift coefficient. This increase is greater the smaller the leading-edge radius or the thinner the airfoil. (See pt. III.) For a cambered airfoil, there is some lift coefficient for which the peak negative pressure is a minimum. Cambered airfoils, particularly those having small values of the leading-edge radius, often have high sharp peaks on the lower surface when operating near zero lift.

The effect of high, sharp, negative-pressure peaks is illustrated in table I, which presents a comparison between estimated and experimentally determined critical speeds for 15 NACA airfoils tested in the NACA 11-inch high-speed tunnel. (See reference 2.) The experimental determination of

TABLE I

COMPARISON OF ESTIMATED WITH EXPERIMENTALLY DETERMINED CRITICAL MACH NUMBERS FOR 15 NACA AIRFOILS

[Experimental values taken from reference 2]

NACA airfoil	At $c_{l_i} = 0$		At $c_{l_i} = 0.2$		At $c_{l_i} = 0.4$	
	Estimated	Experimental	Estimated	Experimental	Estimated	Experimental
0006-62	0.81	0.85	0.61	0.77	0.47	0.62
0012-63	.72	.76	.63	.72	.54	.62
0009-63	.76	.80	.62	.74	.52	.66
0009-62	.70	.73	.62	.69	.54	.60
0009-64	.77	.83	.61	.77	.50	.63
0009-65	.78	.79	.62	.76	.50	.67
0009-66	.77	.77	.62	.73	.50	.63
0009-03	.76	.80	0	.73	0	.68
0009-33	.77	.80	.59	.72	.44	.63
0009-93	.62	.79	.52	.70	.45	.54
0009-05	.81	.82	0	.79	0	.75
0009-35	.81	.80	.53	.77	.39	.69
0009-34	.80	.80	.56	.74	.40	.70
2209-34	.52	.79	.72	.75	.66	.68
2409-34	.62	.78	.73	.74	.69	.71

the critical speed was based on the sharp drag increase occurring at the critical speed. These airfoils were tested at low Reynolds numbers; the chord was only 2 inches. The flow must have been laminar over a considerable portion of the airfoils and would therefore separate in regions of large positive pressure gradient. Every case of serious disagreement between the estimated and the experimental values of the critical Mach number might reasonably be explained as being the result of flow separation. At high Reynolds numbers, the actual critical speeds might therefore be expected, in most cases, to agree more nearly with the estimated values. In cases in which separation is not a factor, the agreement between estimated and experimental critical Mach numbers is almost within the error of the estimation of the critical speeds from the experimental drag values.

Further experimental results are needed to ascertain at what value of the peak negative pressure and for what sharpness of the peak the breakdown of the flow occurs and, when such breakdown of the flow does occur, whether the critical speed corresponds more closely to the actual or to the theoretical peak negative pressure. Such information would be of value especially for estimating the critical speed in a dive, in which case an airfoil designed for lift would be operating near zero lift and might have a high sharp peak on the lower surface near the nose.

The failure of the method in the case of separation of the flow, when the theoretical peak negative pressure coefficients are used for the estimation of the critical speeds, is generally of little practical consequence for the following reasons:

(1) In regard to this type of error, the method is conservative; that is, higher critical speeds are attained than will be estimated.

(2) At high Reynolds numbers, the method will usually be more accurate because with the negative-pressure peak in the most common position near the nose separation will be less likely to occur.

(3) When separation occurs, the flow is usually undesirable from considerations of lift and drag, and the critical speed is no longer required.

It may be concluded that, in general, critical speeds may be estimated with reasonable accuracy from the theoretical peak negative pressures (or from the peak velocities). The method is inaccurate for cases in which high sharp peaks occur, not only because in some instances the theoretical peak may not be attained but also because in others the increase in peak

negative pressure may be somewhat more rapid than indicated by the factor

$$\frac{1}{\sqrt{1 - M_o^2} + \frac{M_o^2 P_1}{2\left(1 + \sqrt{1 - M_o^2}\right)}}$$

Although the critical speeds may, if separation occurs, be estimated considerably too low, they will not ordinarily be estimated much too high. The cases for which the estimation is unsatisfactory are precisely those for which the flow is undesirable because of other considerations.

II. CHARTS FOR USE IN ESTIMATING CRITICAL SPEEDS

In this section are presented charts (figs. 1 to 7) to facilitate the estimation of critical speeds from theoretical low-speed peak negative pressure coefficients $(-P_1)_{max}$. The method is based on the critical Mach number curve given by the approximate relation (7) of part I. The low-speed pressure coefficients P_1 of this curve have been converted to the corresponding velocity coefficients

$$\frac{V_1}{V_o} = \sqrt{1 - P_1}$$

and these coefficients have been plotted against the critical Mach numbers to give the M_{cr} curves of figures 1 to 6. On the same charts are presented peak-velocity coefficients $(V_1/V_o)_{max}$ for a large number of airfoils and, in figure 6, for prolate spheroids and for a few streamline bodies. (See references 17 to 22.) The critical Mach number is estimated simply by moving horizontally from the point representing the peak velocity for the airfoil to the curve M_{cr} then vertically upward to the M_{cr} scale. Such an estimation for the NACA 2415 airfoil at an incompressible-flow lift coefficient of $c_{l_i} = 0.2$ is indicated by the dashed lines in figure 3. The estimated critical Mach number is approximately 0.675. The critical speed may be obtained from the critical Mach number by the relation

$$V_{cr} = M_{cr} \times 49.1\sqrt{460 + t} \text{ feet per second}$$

$$= M_{cr} \times 33.5\sqrt{460 + t} \text{ miles per hour}$$

where t is the air temperature in $^{\circ}F$.

The pressure coefficients P_1, from which the velocity coefficients V_1/V_o used in estimating the critical speeds have been obtained, were computed on the basis of the assumption of potential flow. The

coefficients for two-dimensional flow have been obtained by the method of reference 23. Theoretical pressure distributions for 20 airfoils are given in reference 24. Other distributions can be obtained from references 25 and 26 by the method of reference 26. Reference 27 gives the theory used in computing the pressures over ellipses and prolate spheroids. The pressures over the NACA fuselage form 111 and form 111 modified were computed from a source-sink distribution defining the body (reference 17).

For readers unfamiliar with the system of designating NACA airfoils, a brief explanation will be given here. For the airfoils designated by four digits, such as the NACA 4412 airfoil, the first digit indicates the mean camber in percent of the chord, the second digit gives the position of the maximum camber in tenths of the chord back of the leading edge, and the third and the fourth digits give the maximum thickness in percent of the chord. When the designation has two additional digits preceded by a dash, the first additional digit designates the leading-edge radius; and the second, the location of the maximum thickness in tenths of the chord back of the leading edge. The significance of the leading-edge radius designations is as follows: 0 is a sharp leading edge; 3 is one-fourth normal leading edge; 6 is a normal leading-edge radius; and 9 is three times a normal leading-edge radius or greater. (See reference 2.)

For the 230 series of airfoils (reference 28), the maximum camber is 15 percent of the chord back of the leading edge and the camber has a value such that the ideal angle of attack for the mean line will correspond to a lift coefficient of 0.3. For the charts of the present report, an X in place of one of the shape variables indicates that its value is given along the abscissa scale, the curve holding for all the airfoils in that particular series. As other airfoils or streamline bodies are developed, the corresponding velocity coefficients may be plotted in the charts of figures 1 to 7.

Symmetrical Airfoils at Zero Lift

In figure 1 are presented the peak velocities for a number of symmetrical airfoils at zero lift. This chart will be useful in estimating the critical Mach numbers of struts, fairings, propeller shanks, or any other airfoils operating at zero lift or having a thickness so great that the lift coefficient is a factor of secondary importance. Individual airfoils are indicated by circles. The thickness of the NACA airfoils for which a thickness variation is given is indicated by XX in the designation of the airfoil. Thus, the NACA 0012-63 airfoil is represented by a point on the 00XX-63 curve above 12 on the thickness scale. Peak velocities are given for a typical propeller shank at positions 0.2 and 0.3 of the propeller radius from the hub. These values may be compared with the peak velocities on elliptic cylinders of equal thickness.

For symmetrical airfoils not represented in figure 1, a rough approximation to the peak velocities can be obtained by fitting an ellipse to the airfoil and taking the peak velocity on the equivalent ellipse as equal to that on the airfoil (reference 29). The accuracy of this method obviously depends on how closely the forward portion of the airfoil may be represented by the ellipse. The assumption involved is that the velocities over the forward portion of the airfoil are only slightly affected by the velocities over the rearward portion. The equivalent ellipse may be obtained by assuming that the major axis a is twice the distance from the leading edge of the airfoil to the position of maximum thickness and that the minor axis b is equal to the thickness of the airfoil. The thickness ratio is then

$$\frac{b}{a} = \frac{\text{thickness of airfoil in percent chord}}{\text{twice the position of maximum thickness in percent chord}}$$

The peak velocity may then be obtained from the relation

$$\left(\frac{V_l}{V_o}\right)_{max} = 1 + \frac{b}{a}$$

The critical Mach number may be estimated from the peak velocity by the use of the curve of M_{cr} in figure 1. Table II gives a comparison between peak velocities estimated by this method and those calculated by the more exact theory. The agreement is generally good.

TABLE II

COMPARISON OF PEAK VELOCITIES ON SYMMETRICAL AIRFOILS WITH THOSE OF EQUIVALENT ELLIPSES

Airfoil	Thickness (percent chord)	Location of maximum thickness (percent chord)	Peak velocity, $\left(\frac{V_i}{V_o}\right)_{max}$	
			Estimated from equivalent ellipse	Computed from potential theory
NACA:				
0006-63	6.0	30.0	1.10	1.10
0009-33	9.0	30.0	1.15	1.15
0009-35	9.0	50.0	1.09	1.10
0009-45	9.0	50.0	1.09	1.10
0009-62	9.0	20.0	1.23	1.23
0010-63	10.0	30.0	1.17	1.17
0009-64	9.0	40.0	1.11	1.12
0009-65	9.0	50.0	1.09	1.13
0012-63	12.0	30.0	1.20	1.20
0012-64	12.0	40.0	1.15	1.16
0012-65	12.0	50.0	1.12	1.15
0018-63	18.0	30.0	1.30	1.28
0025-63	25.0	30.0	1.42	1.39
U.S. Navy No. 2 strut[1]	28.6	38.1	1.38	1.37
Rankine struts:[1]				
I	28.5	25.2	1.56	1.47
II	28.6	34.1	1.42	1.41
III	28.5	38.2	1.37	1.37
IV	28.5	33.2	1.43	1.35
V	28.6	40.2	1.36	1.33

[1]See reference 30.

Lifting Airfoils

Figures 2, 3, 4, and 5 are similar to figure 1 but present data for the estimation of critical Mach numbers on airfoils at incompressible-flow lift coefficients of 0, 0.2, 0.4, and 0.6, respectively. Cases in which the peaks are high and sharp, involving such large positive pressure gradients that the computed peak may ordinarily not be attained, are indicated by double circles or dashed lines.

For cambered airfoils, the minimum peak velocity occurs at some lift coefficient other than zero. This lift coefficient of minimum peak velocity corresponds to the theoretical maximum critical speed of the airfoil. Except for the case of symmetrical airfoils, it does not, in general, correspond to the "ideal angle of attack" discussed by Theodorsen and Garrick in reference 23. At the angle of attack corresponding to the minimum peak velocity for a given airfoil, the incompressible-flow lift coefficient will ordinarily be lower than that for which this airfoil is particularly suited because this condition corresponds to a marked negative-pressure peak on the lower surface equal, in fact, to the negative-pressure peak on the upper surface. The lift coefficients of minimum peak velocity for the airfoils included in figures 2 to 5 are presented with the corresponding peak velocities and critical Mach numbers in table III. This table is useful in interpolating between the lift coefficients given in the figures because it indicates the lift coefficient at which the peak velocity changes position from the upper surface to the lower surface; hence, it defines a point of discontinuity in a plot of peak velocity against lift coefficient for a given airfoil. Peak velocities for lift coefficients intermediate between those given by the charts can be obtained by interpolation, if a linear relation is assumed between peak velocity and lift coefficient except when the minimum, given in table III, occurs in the interval. In such a case, the value of $(V_i/V_o)_{max}$ will be obtained by interpolation each way from the minimum.

TABLE III

PEAK VELOCITY AND CRITICAL SPEED AT THE

INCOMPRESSIBLE-FLOW LIFT COEFFICIENT OF MINIMUM PEAK VELOCITY

Airfoil	Lift coefficient, c_{l_i}	Peak velocity, $\left(\frac{V_i}{V_o}\right)_{max}$	Estimated critical Mach number, M_{cr}	Airfoil	Lift coefficient, c_{l_i}	Peak velocity, $\left(\frac{V_i}{V_o}\right)_{max}$	Estimated critical Mach number, M_{cr}
NACA:							
23009	0.10	1.24	0.69	Boeing 103A, 10.5	0.24	1.24	0.69
23012	.08	1.27	.67	R.A.F. 15, 10.5	.26	1.26	.67
23018	-.06	1.27	.67	R.A.F. 19, 10.5	.95	1.52	.54
23012-64	.09	1.24	.69	Göttingen 398, 13.75	.38	1.37	.61
2209-34	.15	1.19	.73	Göttingen 387, 14.85	.50	1.41	.59
2209	.22	1.23	.70	NACA - M6, 12	.11	1.25	.68
2212	.11	1.25	.68	N-22, 12.37	.34	1.32	.64
2215	.09	1.28	.66	U.S.A. 27, 11.12	.47	1.37	.61
2218	.09	1.31	.64	U.S.A. 35B, 11.61	.32	1.30	.65
2409-34	.11	1.17	.75	Clark Y propeller sections:			
2409	.22	1.20	.72	6	.22	1.19	.73
2412	.17	1.21	.71	9	.24	1.22	.70
2415	.17	1.25	.68	11.7	.28	1.27	.67
4412	.36	1.29	.65	18	.41	1.38	.60
6512	.59	1.35	.62	Clark Y double-camber Navy design 5868 at $\frac{r}{R}$ = 0.4, 17.5	.50	1.42	.58
Clark Y M,18[a]	.27	1.35	.62				
Clark Y M,15	.28	1.31	.64				
Clark Y M, 9	.37	1.24	.69				
NACA CYH, 18	.11	1.31	.64	R.A.F. 6 propeller sections:			
NACA CYH, 11.7	.16	1.28	.66				
C-72, 11.85	.32	1.27	.67	6	.25	1.22	.70
				9	.38	1.31	.64
				15	.54	1.42	.58

[a]The number after the comma in the following airfoil designations indicates the thickness of the airfoil in percent chord.

Some difficulty may be experienced in arriving at the proper value of c_{l_i} for use in the charts. With a given angle of attack the lift coefficient may be assumed to increase with Mach number according to the Glauert factor $1/\sqrt{1 - M_o^2}$ (reference 9). The true lift coefficients corresponding to the incompressible-flow values c_{l_i} given in the charts are then

$$c_l \approx \frac{c_{l_i}}{\sqrt{1 - M_o^2}} \tag{8}$$

If a value of c_l be assumed, this relation may be used with figures 2 to 5 and table III to make a simple plot of M_o and M_{cr} against c_{l_i}. The intersection of the two curves gives c_{l_i} and the corresponding value of M_{cr}. It will usually be sufficient, however, to use c_l in the charts to obtain an approximate value of M_{cr} that may be inserted in (8) to give a value of c_{l_i} for a second approximation.

If the wing loading W/S is fixed, c_{l_i} is a somewhat more complicated function of the Mach number. Thus

$$c_l = \frac{2\frac{W}{S}}{\rho_o V_o^2}$$

where W/S must be taken as the wing loading pertaining to the particular section being investigated, and with $V_o = M_o a_o$, (8) gives

$$c_{l_i} \approx \frac{2\frac{W}{S}}{\rho_o a_o^2} \frac{\sqrt{1 - M_o^2}}{M_o^2} \tag{9}$$

With the given value of W/S and values of ρ_o and a_o corresponding to the existing temperature and pressure, M_o may then be plotted against c_{l_i}; and, with M_{cr} from figures 2 to 5 and table III plotted against c_{l_i} on the same scale, the required values of c_{l_i} and M_{cr} are given by the intersection of the two curves.

Streamline Bodies and Interference

In figure 6 are presented peak velocities on prolate spheroids and certain other bodies of revolution. Except for the prolate spheroids and NACA fuselage form 111, the peak velocities have been obtained from

measured pressure distributions. In a manner similar to that suggested for symmetrical airfoils, the peak velocity on a streamline body may be approximated from the peak velocity of the prolate spheroid that can be most nearly fitted to the forward part of the streamline body. The curve for elliptic cylinders has been included for comparison with the prolate spheroids. The induced velocity on a three-dimensional body is seen to be less than half that on the corresponding two-dimensional body and the ratio to decrease as the fineness ratio increases. A curve for the prolate spheroids at 6° angle of attack is included to show the increase in peak velocity with angle of attack. The computed effect is small, though a much larger effect was found experimentally for the U.S. airship Akron. From the given peak velocities, the critical Mach numbers for bodies of revolution can be estimated. The critical speeds of three-dimensional bodies will generally be much higher than the critical speeds of two-dimensional bodies.

When two aerodynamic bodies are operating close together, the critical speed of the combination may be lower than that of either body operating alone because each is influenced by the velocity field of the other. A rough approximation to the critical speed of the combination may be obtained by considering the body having the lower critical speed to be operating in a velocity field given by

$$\frac{V}{V_o} = 1 + \frac{\Delta V}{V_o}$$

where $\Delta V/V_o$ is the induced, or excess, velocity, expressed as a fraction of the forward velocity V_o, due to the other body. For small (usual) values of the velocity ratio, a good approximation to the effect of compressibility is given by multiplying the induced velocity by the factor $1\Big/\sqrt{1 - M_o^2}$. Thus

$$\frac{\Delta V}{V_o} = \frac{1}{\sqrt{1 - M_o^2}} \frac{\Delta V_1}{V_o}$$

The critical speed of the combination is then given by

$$\text{Critical Mach number of combination} = \frac{M_{cr}}{1 + \frac{\Delta V}{V_o}}$$

where

$$\frac{\Delta V}{V_o} = \frac{1}{\sqrt{1 - M_{cr}^2}} \frac{\Delta V_1}{V_o}$$

and M_{cr} is the critical Mach number of the body having the lowest critical speed, usually the wing. (See figs. 1 to 6.) The value M_o in the factor $1/\sqrt{1 - M_o^2}$ should strictly be somewhat less than M_{cr} but the error involved in using M_{cr} is small and conservative. If several bodies contribute interference, $\Delta V_i/V_o$ may be taken as the sum of the interfering velocities:

$$\frac{\Delta V_i}{V_o} = \left(\frac{\Delta V_i}{V_o}\right)_1 + \left(\frac{\Delta V_i}{V_o}\right)_2 + \cdots$$

For bodies operating behind the propeller, the effect of the slipstream may be included by adding the excess velocity $\Delta V/V_o$ due to the slipstream at high-speed operating conditions directly to the excess velocity $\Delta V/V_o$ due to the interference.

In the estimation of the interference velocities due to a body at a distance, an additional compressibility effect may be included by expanding the field of the interfering body in a direction normal to the flow in the ratio $1/\sqrt{1 - M_o^2}$ (see reference 8) or otherwise, for the estimation from incompressible-flow data, decreasing the distance by the factor $\sqrt{1 - M_o^2}$. The effect of this correction on the estimated critical Mach number will usually be insignificant but, if it is to be applied, an approximate critical Mach number obtained without consideration of this correction may be used for estimating the expansion of the field.

Interference and slipstream velocities often operate to change the lift coefficient of the wing section subject to the interference, but the effect is assumed to be sufficiently small that the change in angle of attack of the airplane is negligible.

The method outlined has not yet been fully justified by experiment and may not, in every case, be conservative; but, pending further results of experiment, it should serve for a rough approximation of the effect of interference on the critical speed. If pressure distributions are available for nacelles, cowlings, windshields, or other bodies, they may be converted into induced velocity coefficients by the low-speed relation between induced velocity coefficients and pressure coefficients

$$\frac{\Delta V_i}{V_o} = \sqrt{1 - P_i} - 1$$

The peak velocities may then be used either to estimate the interference of the body on the airfoil and the critical speed of the combination or

to predict the critical speed of the body alone. For blunt bodies, such as cowlings and windshields, the critical speed may be lower than that of the wing and it may be desirable to estimate the interference effect of the wing on the critical speed of the body. For many bodies, the peak velocities may be estimated directly from figure 6. For an estimation of the interference effect at a distance from the surface of a body, figure 7 shows the decay of velocities with distance in the median plane of prolate spheroids and elliptic cylinders.

The method of estimating critical Mach numbers when interference is present will be demonstrated by an example.

Assume a two-engine monoplane of the following characteristics:

Wing loading, pounds/square foot	32
Wing profile at fuselage	NACA 23018
Wing profile at nacelle	NACA 23016
Fuselage width, inches	48
Fuselage length, inches	480
Distance from airplane center line to nacelle center line, inches	108
Nacelle diameter, inches	56
Operating altitude, feet	20,000
Density ratio	0.5327
Velocity of sound, miles per hour	709
Velocity of sound, feet per second	1040

The fuselage fineness ratio is 10 in plan view and 8 in elevation. The induced velocity at the wing-fuselage juncture due to the fuselage is estimated to be the same as for a prolate spheroid of fineness ratio 6. The induced velocity at the nacelle-wing juncture due to the nacelle is estimated to be the same as for a prolate spheroid of fineness ratio 2.5. The corresponding induced velocity (fig. 7) is 0.15 and the corresponding pressure coefficient, approximately $P = -0.3$, agrees with values commonly found on the central part of nacelles.

At the wing-fuselage juncture, the maximum induced velocity due to the fuselage (fig. 7, fineness ratio = 6, $x/D = 0.5$; or see fig. 6) is 0.05 and that due to the nacelle (fig. 7, fineness ratio = 2.5, $x/D = (108 - 24)/56 = 1.50$) is 0.025. The critical Mach number for the NACA 23018 airfoil is estimated from figures 2 and 3 as follows:

M_{cr} wing alone for $c_{l_i} = 0$ 0.650

M_{cr} wing alone for $c_{l_i} = 0.2$ 0.605

Fuselage $\Delta V_i/V_o$ 0.05
Nacelle $\Delta V_i/V_o$ 0.025
Fuselage + nacelle $\Delta V_i/V_o$ 0.075

Fuselage + nacelle $\Delta V/V_o$ for $c_{l_i} = 0 \left(= \frac{0.075}{\sqrt{1 - 0.650^2}} \right)$ 0.099

Fuselage + nacelle $\Delta V/V_o$ for $c_{l_i} = 0.2 \left(= \frac{0.075}{\sqrt{1 - 0.605^2}} \right)$ . . . 0.094

M_{cr} wing + fuselage + nacelle for $c_{l_i} = 0 \left(= \frac{0.650}{1 + 0.099} \right)$ . . . 0.592

M_{cr} wing + fuselage + nacelle for $c_{l_i} = 0.2 \left(= \frac{0.605}{1 + 0.094} \right)$ . . 0.553

With values of M_o chosen near the values of M_{cr}, corresponding values of c_{l_i} from equation (9) are

c_{l_i} for $M_o = 0.60 \left(= \frac{2 \times 32}{0.002378 \times 0.5327 \times 1040^2} \frac{\sqrt{1-0.60^2}}{0.60^2} \right)$ 0.104

c_{l_i} for $M_o = 0.56 \left(= \frac{2 \times 32}{0.002378 \times 0.5327 \times 1040^2} \frac{\sqrt{1-0.56^2}}{0.56^2} \right)$ 0.124

The intersection of the M_o and the M_{cr} lines in figure 8(a) gives the required critical Mach number

$$M_{cr} = 0.57$$

and the corresponding critical speed at 20,000 feet

$$V_{cr} = 0.57 \times 709 = 404 \text{ miles per hour}$$

The approximate critical speed thus obtained could be used to reduce the distance to the nacelle from $x/D = 1.5$ to an effective distance $\left(\frac{x}{D}\right)_{eff} = 1.5 \times \sqrt{1 - 0.57} = 1.32$ and, from figure 7, the coefficient

of the interference velocity due to the nacelle would be 0.030 instead of 0.025. The corresponding value of the critical Mach number is 0.567, but the accuracy of the method is insufficient to justify this correction.

At the inboard wing-nacelle juncture, the maximum induced velocity due to the nacelle (fig. 7, fineness ratio = 2.5, x/D = 0.5; or see fig. 6) is 0.15 and that due to the fuselage (fig. 7, fineness ratio = 6, x/D = (108 - 28)/48 = 1.67) is 0.015. The induced velocity in the slipstream at high speed is assumed to be 0.04. The critical Mach number at this point on the wing is then:

M_{cr} wing alone for $c_{l_i} = 0$ 0.668

M_{cr} wing alone for $c_{l_i} = 0.2$ 0.613

Nacelle $\Delta V_i/V_o$ 0.15

Fuselage $\Delta V_i/V_o$ 0.015

Nacelle + fuselage $\Delta V_i/V_o$ 0.165

Nacelle + fuselage $\Delta V/V_o$ for $c_{l_i} = 0 \left(= \frac{0.165}{\sqrt{1 - 0.668^2}}\right)$ 0.222

Nacelle + fuselage $\Delta V/V_o$ for $c_{l_i} = 0.2 \left(= \frac{0.165}{\sqrt{1 - 0.613^2}}\right)$ 0.209

Slipstream $\Delta V/V_o$ 0.040

M_{cr} wing + nacelle + fuselage + slipstream for $c_{l_i} = 0 \left(= \frac{0.668}{1+0.22+0.04}\right)$ 0.529

M_{cr} wing + nacelle + fuselage + slipstream for $c_{l_i} = 0.2 \left(= \frac{0.613}{1+0.209+0.04}\right)$ 0.491

From relation (9),

c_{l_i} for $M_o = 0.53$ 0.141

c_{l_i} for $M_o = 0.49$ 0.170

The plot of M_o and M_{cr} against c_{l_i} in figure 8(b) shows

$$M_{cr} = 0.50$$

V_{cr} at 20,000 feet = 0.50 × 709 = 355 miles per hour

The critical point on the wing is therefore the nacelle-wing juncture. Because this critical region is small, however, the drag increase will be

less serious at the corresponding critical Mach number than if the breakdown of the flow had occurred over a larger part of the wing.

III. EFFECT OF VARIOUS AIRFOIL SHAPE CHARACTERISTICS

From the foregoing charts and discussion, it is apparent that high critical speeds correspond to low peak negative pressure (or velocity) coefficients. As a partial answer to the question of just what kind of airfoil is best for high speeds, a brief and necessarily incomplete analysis and discussion of airfoil shape characteristics in relation to critical speeds will be presented.

Because of the required pressure difference between upper and lower surfaces of the wing the critical speed must, in general, necessarily decrease with increase in the absolute value of the lift coefficient; but this effect is often masked by the effect of the large additional pressures that appear near the nose when, either through angle-of-attack change or through camber, the nose angle of attack becomes different from zero. A negative-pressure peak near the nose may often be relieved by a change in camber, and the airfoil may thus be rendered more suitable for use at the given lift coefficient. This fact is illustrated in the charts (figs. 2 to 5) where, as the lift coefficient is increased, the more highly cambered airfoils show the lowest velocity coefficients and the highest critical speeds.

One of the most important shape characteristics is thickness. The influence of thickness is evident from the curves of figures 1 to 6. Except where some other characteristic - such as camber or leading-edge radius - is effective, the induced velocity at constant angle of attack is almost a linear function of thickness. This result might have been expected from the results for the elliptic cylinder, for which the maximum induced velocity coefficient at zero lift is equal to the thickness ratio. The rate of increase of velocity with thickness is generally somewhat greater for airfoils than for elliptic cylinders because of the necessity for a streamline tail. As the thickness is increased, the airfoil becomes less sensitive to other characteristics and, for very thick airfoils, the peak velocity is determined largely by the thickness.

Figure 9 shows the influence of the position of maximum thickness, which is indicated in the airfoil designation by X. For symmetrical airfoils at zero lift, the highest critical speed is attained if the position of maximum thickness is about 50 percent of the chord from the leading edge. This condition should also be true for cambered airfoils operating near the best lift coefficient. The curve of figure 9 through the points for the NACA 23012-63 and the NACA 23012-64 airfoils at $c_{l_i} = 0.1$ indicates this trend.

The effect of camber is shown in figure 10, where each airfoil is represented at the lift coefficient of minimum peak velocity. As would be expected from the fact that the lift coefficient corresponding to minimum peak velocity increases as the camber is increased (see fig. 11), the velocity coefficient is increased by camber. Figure 10 also indicates that the effects of camber are less marked on thick airfoils and that thin airfoils are particularly sensitive to changes of camber.

Figure 12 shows the effect of the position of maximum camber on the velocity coefficient for the lift coefficient of minimum peak velocity of several NACA airfoils. Thus, the decreasing velocity coefficient with rearward movement of the maximum-camber position is partly due to the fact that the lift coefficient corresponding to minimum peak velocity becomes less; but other considerations indicate that this trend is the same if the lift coefficient is eliminated as a variable, so that camber positions forward of the 40-percent-chord point are not to be recommended for high-speed airfoils.

Another characteristic affecting the critical speed is the leading-edge radius. The significance of the index of the leading-edge radius as well as of the other numbers designating the variables in the airfoils of the NACA series is explained in reference 2. The leading-edge radius is particularly important if the airfoil is to be operated at an angle of attack different from the ideal (reference 31). If the leading-edge radius is too small (say, near index 3), high, sharp, negative-pressure peaks will be built up on the leading edge when the angle of attack varies considerably from the ideal. If, on the other hand, the index of the leading-edge radius is greater than about 6, a negative-pressure peak may occur on the leading edge at or near the ideal angle of attack. A somewhat larger index may be permissible for thick airfoils than for thin ones. Figure 13 indicates that, for the 9-percent-thick symmetrical airfoils at zero lift, an index near 4 gives the lowest peak velocities. Further investigation, taking account of the maximum lift as well as of the peak negative pressures over the angle-of-attack range, is needed to determine what leading-edge radius is most satisfactory for airfoils to be used in high-speed operation.

CONCLUDING REMARKS

Critical compressibility speeds can, in most cases, be satisfactorily estimated from pressure or velocity distributions not only for two-dimensional but also for three-dimensional flow. The relation between peak velocity and critical Mach number is given, together with the necessary peak-velocity data for a large number of airfoils and streamline bodies, so that the critical Mach numbers can be conveniently estimated directly from the charts. A method is introduced to allow for the interference from other bodies, thus permitting a closer approximation to the critical speed of the combination of wing, fuselage, and nacelles

than would otherwise be obtained. Because the method of allowing for interfering velocities may not in every case be conservative, ample margin should be allowed in the design of parts subject to such interference. Pending further investigation, the method should, however, furnish a satisfactory engineering approximation to the effect of interference velocities on the critical speed.

The critical speed of an airfoil is determined by the thickness, the thickness distribution, the camber, the camber distribution, the leading-edge radius, and the lift coefficient at which the airfoil operates at high speeds. For high critical speeds, the positions of maximum thickness and maximum camber should be in the vicinity of the 50-percent-chord point, and the camber should be chosen for the lift coefficient at which the high-speed operation will occur.

Langley Memorial Aeronautical Laboratory,
National Advisory Committee for Aeronautics,
Langley Field, Va.

REFERENCES

1. Stack, John: The N.A.C.A. High-Speed Wind Tunnel and Tests of Six Propeller Sections. NACA Rep. No. 463, 1933.

2. Stack, John, and von Doenhoff, Albert E.: Tests of 16 Related Airfoils at High Speeds. NACA Rep. No. 492, 1934.

3. Stack, John, Lindsey, W. F., and Littell, Robert E.: The Compressibility Burble and the Effect of Compressibility on Pressures and Forces Acting on an Airfoil. NACA Rep. No. 646, 1938.

4. Jacobs, Eastman N.: Methods Employed in America for the Experimental Investigation of Aerodynamic Phenomena at High Speeds. NACA Misc. Paper No. 42, 1936.

5. Taylor, G. I., and Maccoll, J. W.: The Mechanics of Compressible Fluids. Vol. III of Aerodynamic Theory, div. H, W. F. Durand, ed., Julius Springer (Berlin), 1935, pp. 210-250.

6. Stack, John: The Compressibility Burble. NACA TN No. 543, 1935.

7. Ferri, Antonio: Investigations and Experiments in the Guidonia Supersonic Wind Tunnel. NACA TM No. 901, 1939.

8. Ackeret, J.: Über Luftkräfte bei sehr grossen Geschwindigkeiten insbesondere bei ebenen Strömungen. Helvetica Physica Acta, vol. I, fasc. 5, 1928, pp. 301-322.

9. Glauert, H.: The Effect of Compressibility on the Lift of an Aerofoil. R. & M. No. 1135, British A.R.C., 1927.

10. von Kármán, Th.: Compressibility Effects in Aerodynamics. Jour. Aero. Sci., vol. 8, no. 9, July 1941, pp. 337-356.

11. Robinson, Russell G., and Becker, John V.: High-Speed Tests of Conventional Radial-Engine Cowlings. NACA Rep. No. 745, 1942.

12. Kaplan, Carl: Two-Dimensional Subsonic Compressible Flow past Elliptic Cylinders. NACA Rep. No. 624, 1938.

13. Kaplan, Carl: Compressible Flow about Symmetrical Joukowski Profiles. NACA Rep. No. 621, 1938.

14. Stanton, T. E.: On the Distribution of Pressure over a Symmetrical Joukowski Section at High Speeds. R. & M. No. 1280, British A.R.C., 1930.

15. Lees, Lester: A Discussion of the Application of the Prandtl-Glauert Method to Subsonic Compressible Flow over a Slender Body of Revolution. NACA TN No. 1127, 1946.

16. Kaplan, Carl: The Flow of a Compressible Fluid past a Sphere. NACA TN No. 762, 1940.

17. Abbott, Ira H.: Fuselage-Drag Tests in the Variable-Density Wind Tunnel: Streamline Bodies of Revolution, Fineness Ratio of 5. NACA TN No. 614, 1937.

18. Jones, R., and Williams, D. H.: The Distribution of Pressure over the Surface of the Airship Model U.721, Together with a Comparison with the Pressure over a Spheroid. R. & M. No. 600, British A.C.A., 1919.

19. Freeman, Hugh B.: Pressure-Distribution Measurements on the Hull and Fins of a 1/40-Scale Model of the U.S. Airship "Akron." NACA Rep. No. 443, 1932.

20. Lyon, H. M.: A Study of the Flow in the Boundary Layer of Streamline Bodies. R. & M. No. 1622, British A.R.C., 1935.

21. Lock, C. N. H., and Johansen, F. C.: Drag and Pressure-Distribution Experiments on Two Pairs of Streamline Bodies. R. & M. No. 1452, British A.R.C., 1933.

22. Ower, E., and Hutton, C. T.: Investigation of the Boundary Layers and the Drags of Two Streamline Bodies. R. & M. No. 1271, British A.R.C., 1930.

23. Theodorsen, T., and Garrick, I. E.: General Potential Theory of Arbitrary Wing Sections. NACA Rep. No. 452, 1933.

24. Garrick, I. E.: Determination of the Theoretical Pressure Distribution for Twenty Airfoils. NACA Rep. No. 465, 1933.

25. Jacobs, Eastman N., and Rhode, R. V.: Airfoil Section Characteristics as Applied to the Prediction of Air Forces and Their Distribution on Wings. NACA Rep. No. 631, 1938.

26. Allen, H. Julian: A Simplified Method for the Calculation of Airfoil Pressure Distribution. NACA TN No. 708, 1939.

27. Zahm, A. F.: Flow and Drag Formulas for Simple Quadrics. NACA Rep. No. 253, 1927.

28. Jacobs, Eastman N., and Clay, William C.: Characteristics of the N.A.C.A. 23012 Airfoil from Tests in the Full-Scale and Variable-Density Tunnels. NACA Rep. No. 530, 1935.

29. Hooker, S. G.: The Two-Dimensional Flow of Compressible Fluids at Sub-Sonic Speeds past Elliptic Cylinders. R. & M. No. 1684, British A.R.C., 1936.

30. Smith, R. H.: Aerodynamic Theory and Test of Strut Forms - II. NACA Rep. No. 335, 1929.

31. Theodorsen, Theodore: On the Theory of Wing Sections with Particular Reference to the Lift Distribution. NACA Rep. No. 383, 1931.

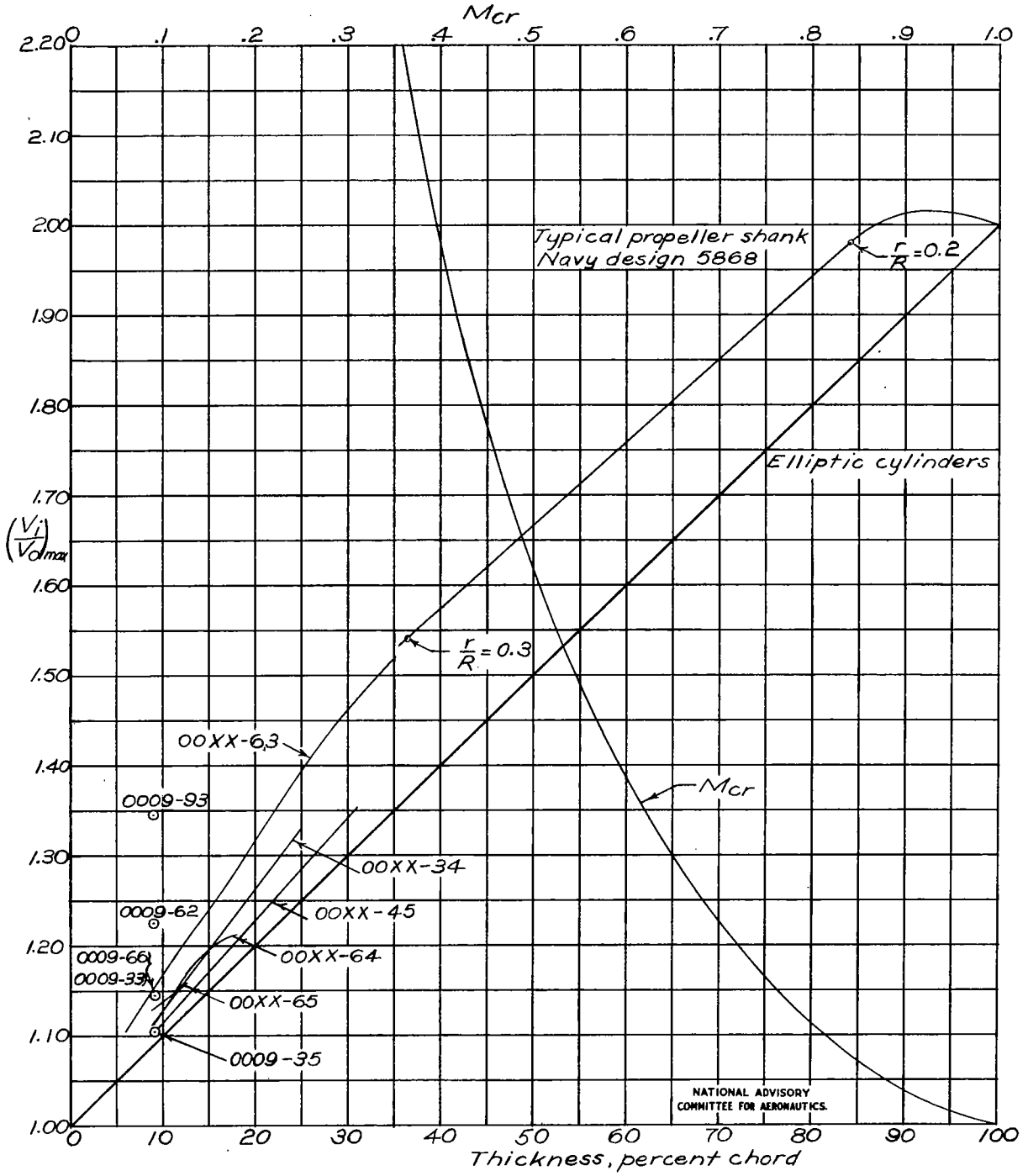

Figure 1. — Peak velocities and critical speeds for symmetrical airfoils at zero lift. Airfoils designated only by numbers belong to the NACA family.

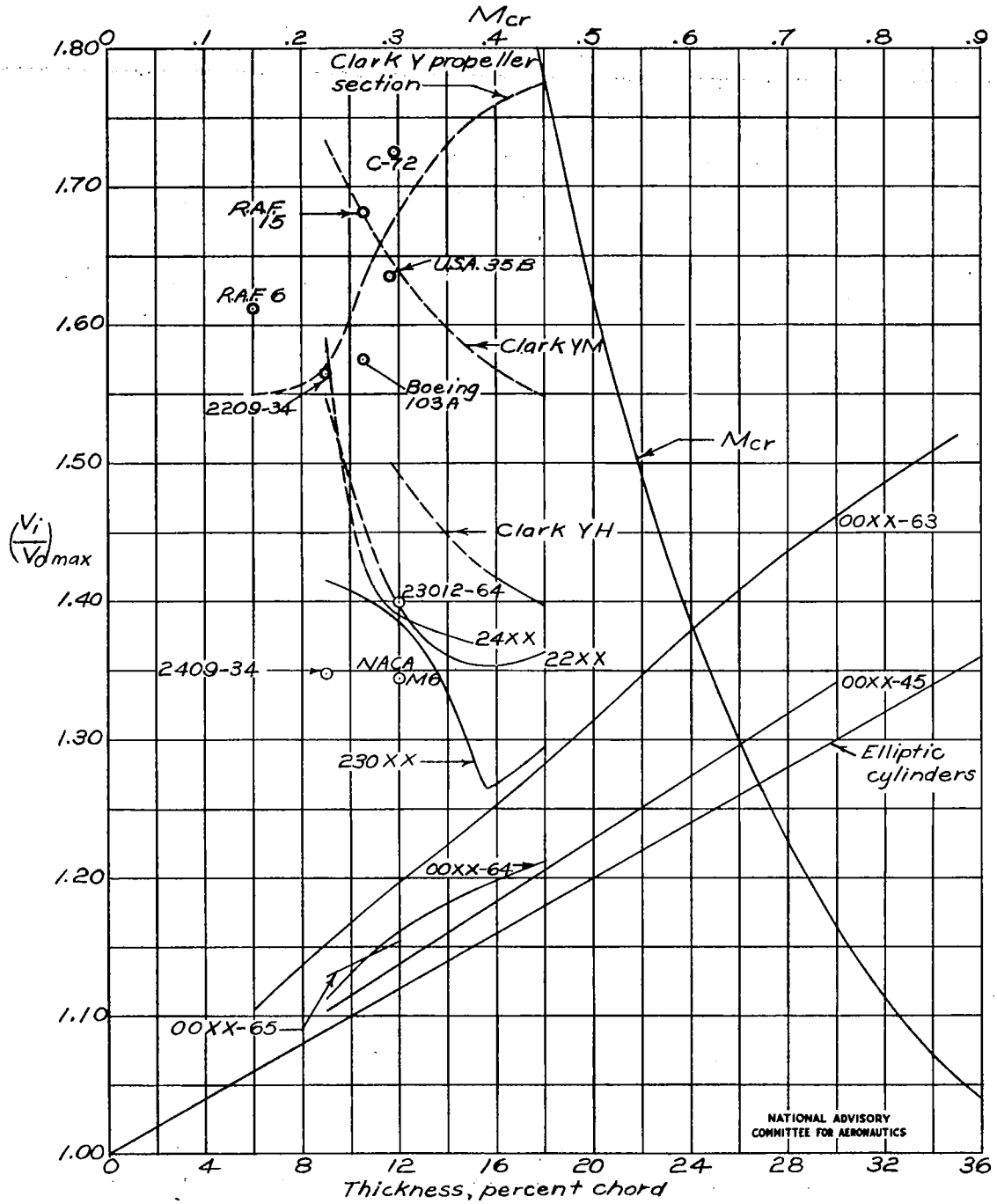

Figure 2.— Peak velocities and critical speeds for airfoils at $C_{l_i} = 0$. Double circle or dashed line denotes that actual value of peak velocity may be less than indicated. Airfoils designated only by numbers belong to the NACA family.

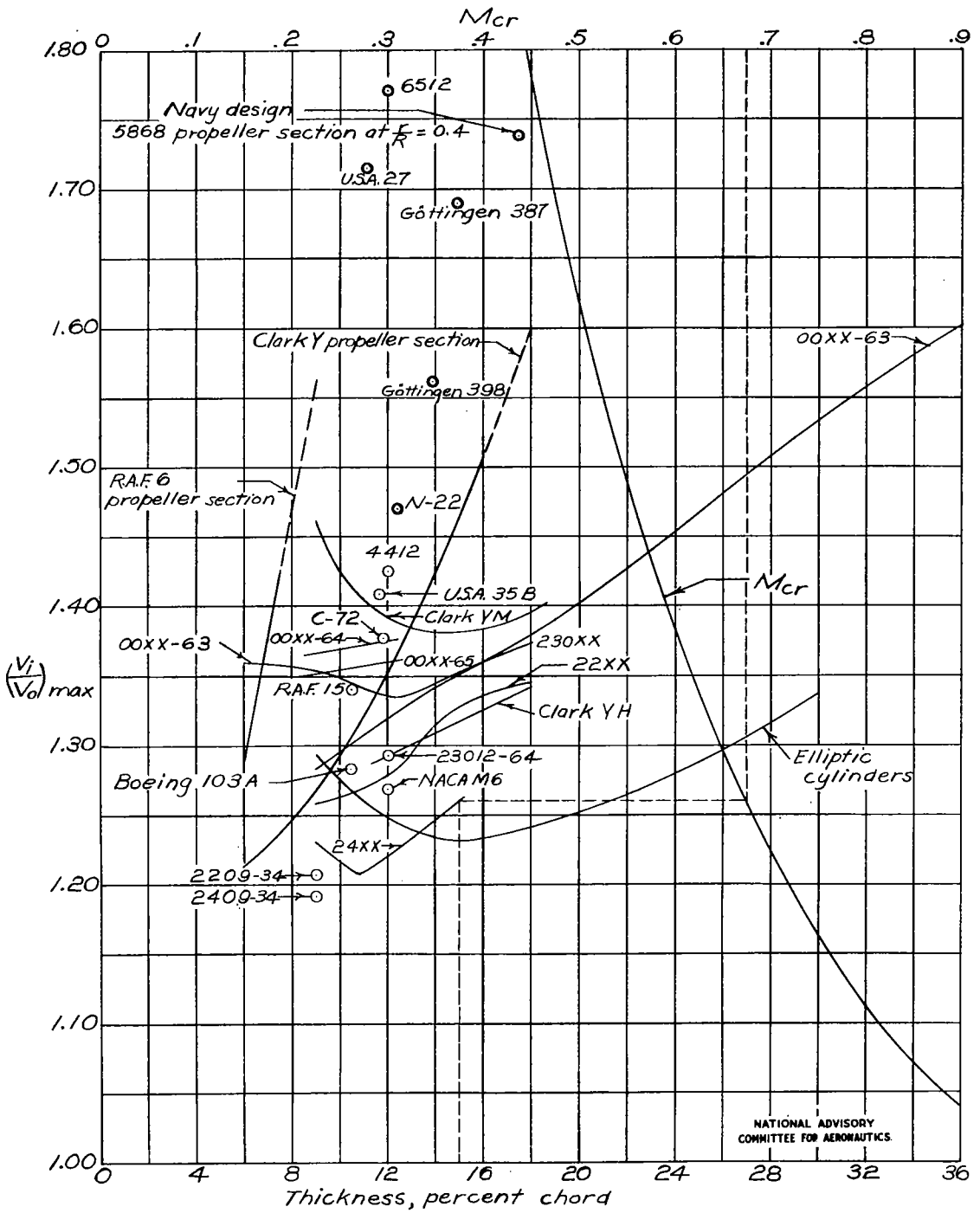

Figure 3. — Peak velocities and critical speeds for airfoils at $C_{l_i} = 0.2$. Double circle or dashed line denotes that actual value of peak velocity may be less than indicated. Airfoils designated only by numbers belong to the NACA family.

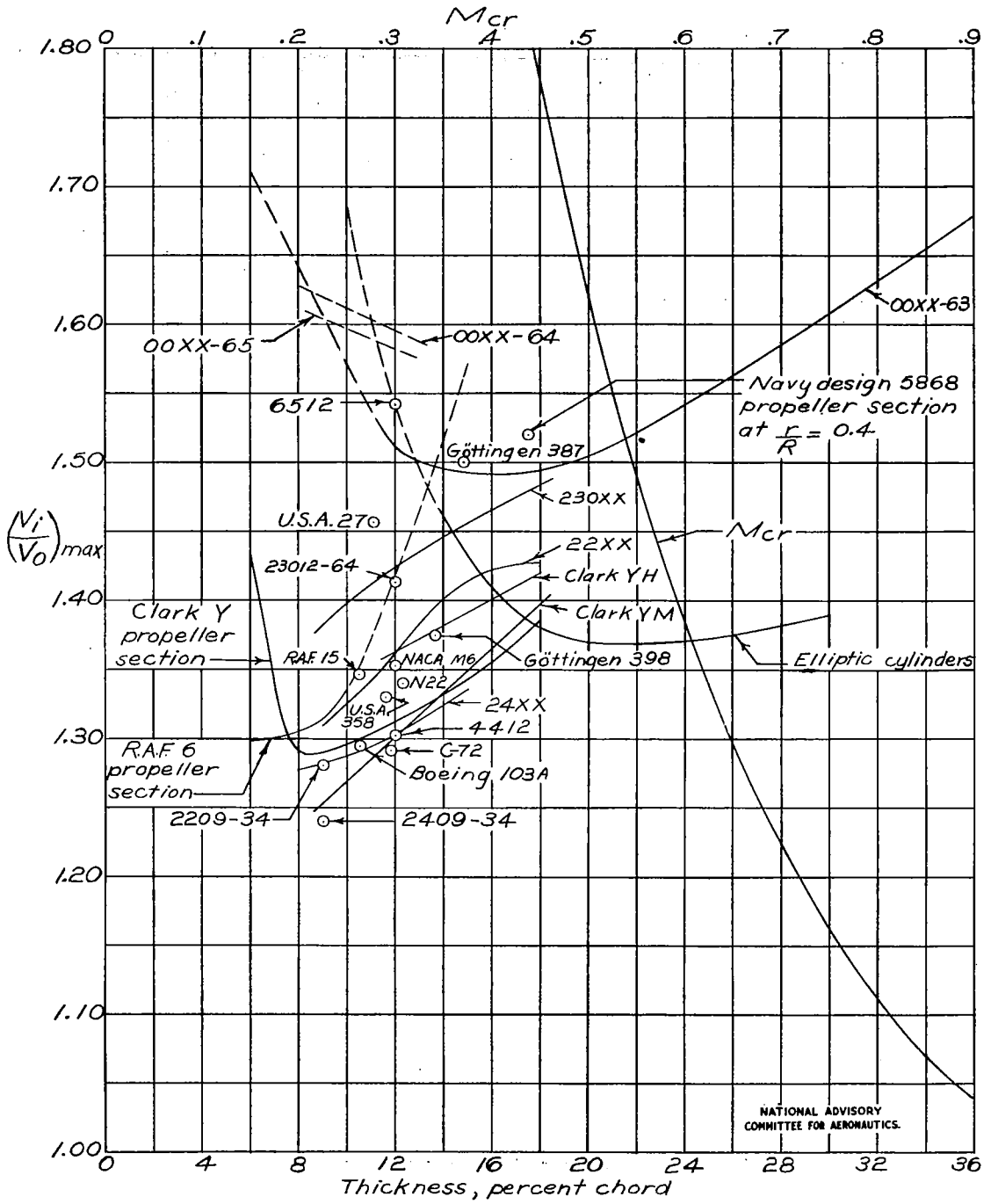

Figure 4. — Peak velocities and critical speeds for airfoils at $C_{l_i} = 0.4$. Dashed line denotes that actual value of peak velocity may be less than indicated. Airfoils designated only by numbers belong to the NACA family.

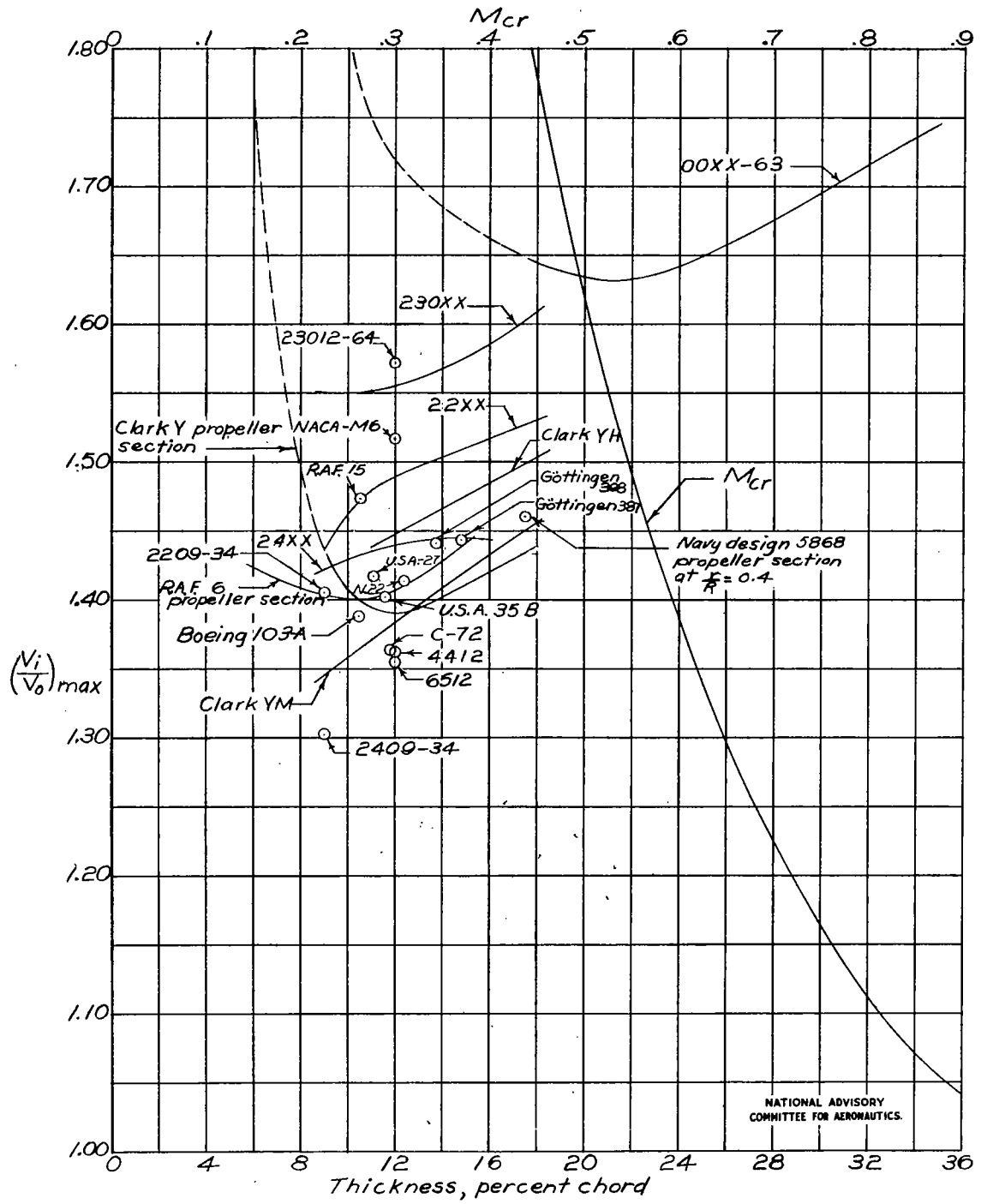

Figure 5 .— Peak velocities and critical speeds for airfoils at $C_{l_i} = 0.6$. Dashed line denotes that actual value of peak velocity may be less than indicated. Airfoils designated only by numbers belong to the NACA family.

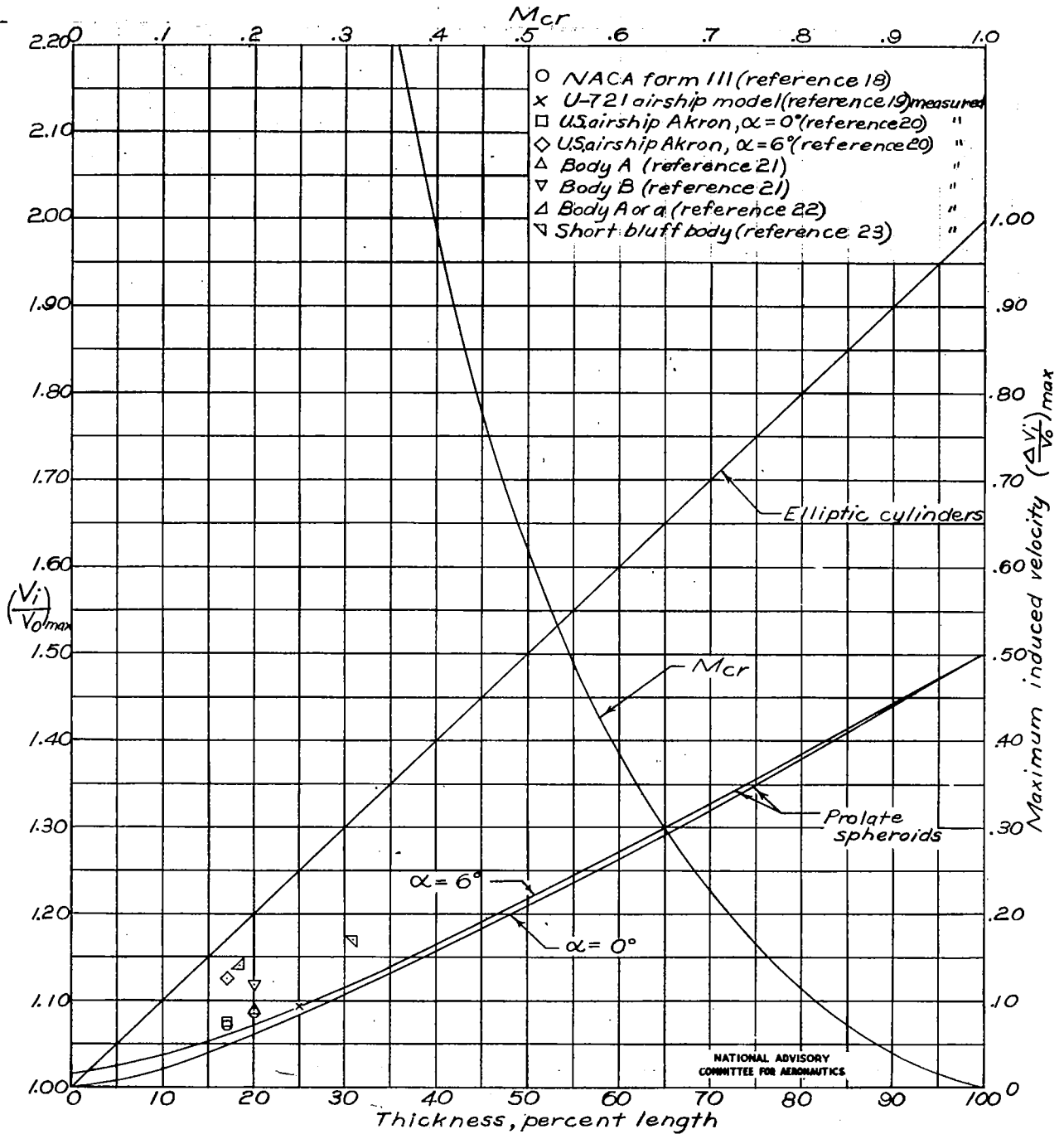

Figure 6. — Peak velocities and critical speeds for bodies of revolution.

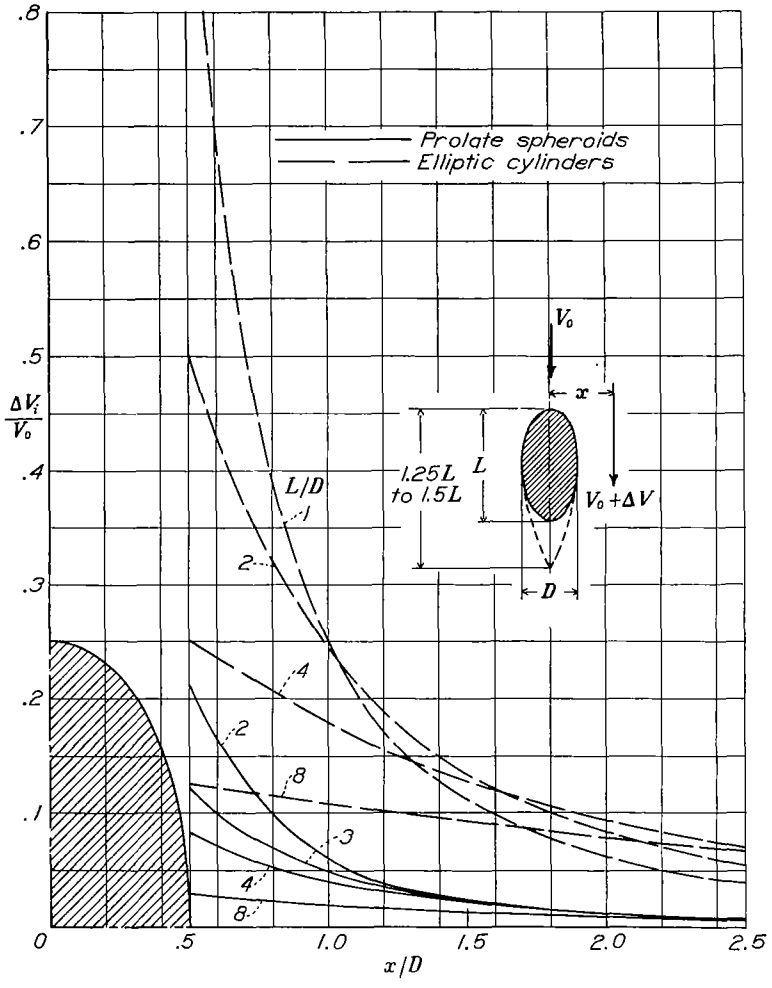

Figure 7.- Decay of velocity in the median plane of prolate spheroids and elliptic cylinders.

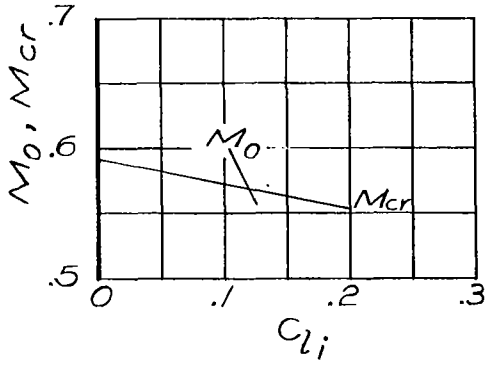

(a)

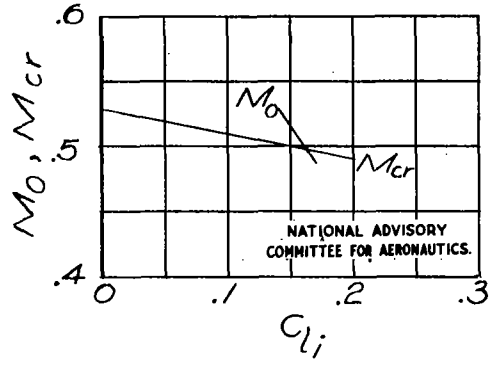

(b)

Figure 8. — Determination of critical Mach number for an airfoil with given lift loading from intersection of curves of Mach number and critical Mach number above incompressible-flow lift coefficients.

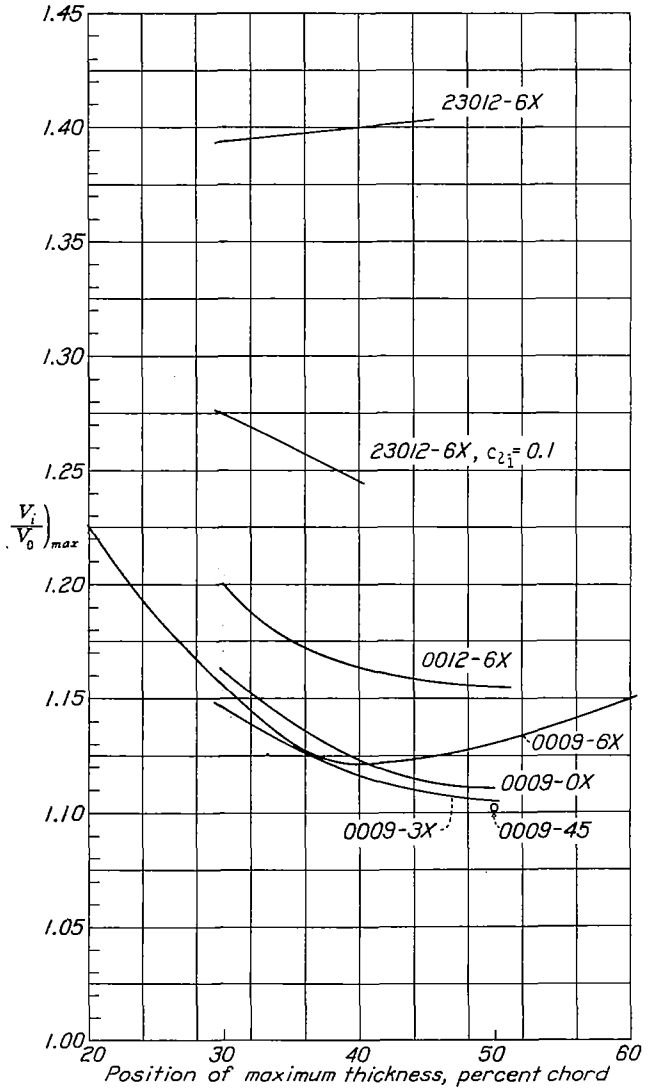

Figure 9.- Variation of peak velocities with position of maximum thickness. c_{l_i}= 0 except as otherwise noted. Airfoils belong to the N.A.C.A. family.

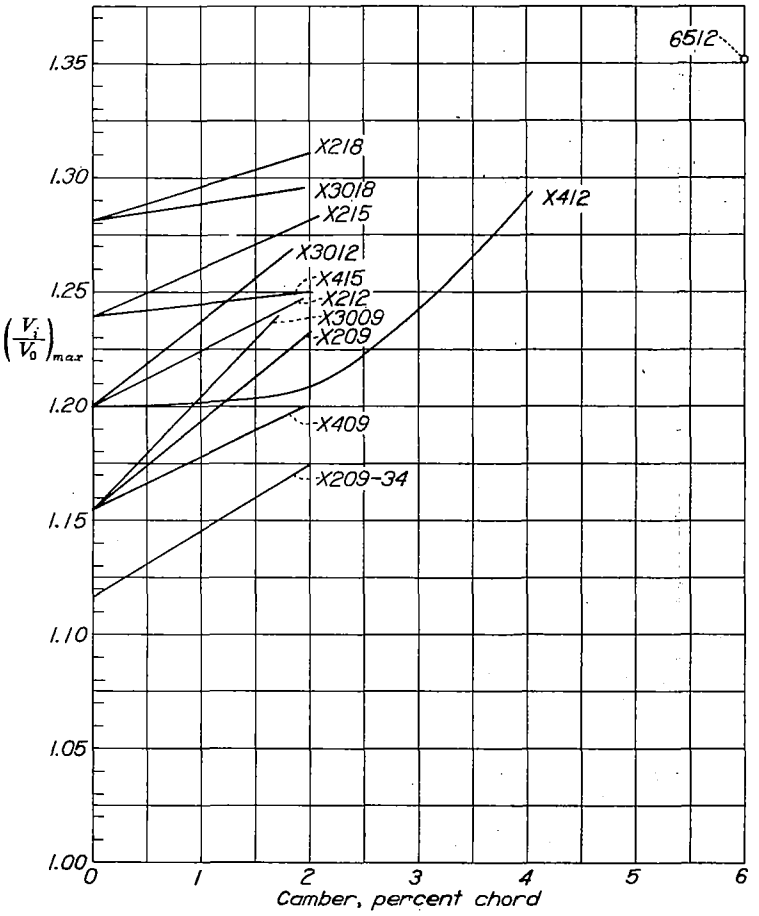

Figure 10.- Variation of peak velocities with camber. The value of c_{l_i} in each case is that for which the peak velocity is a minimum. Airfoils belong to the N.A.C.A. family.

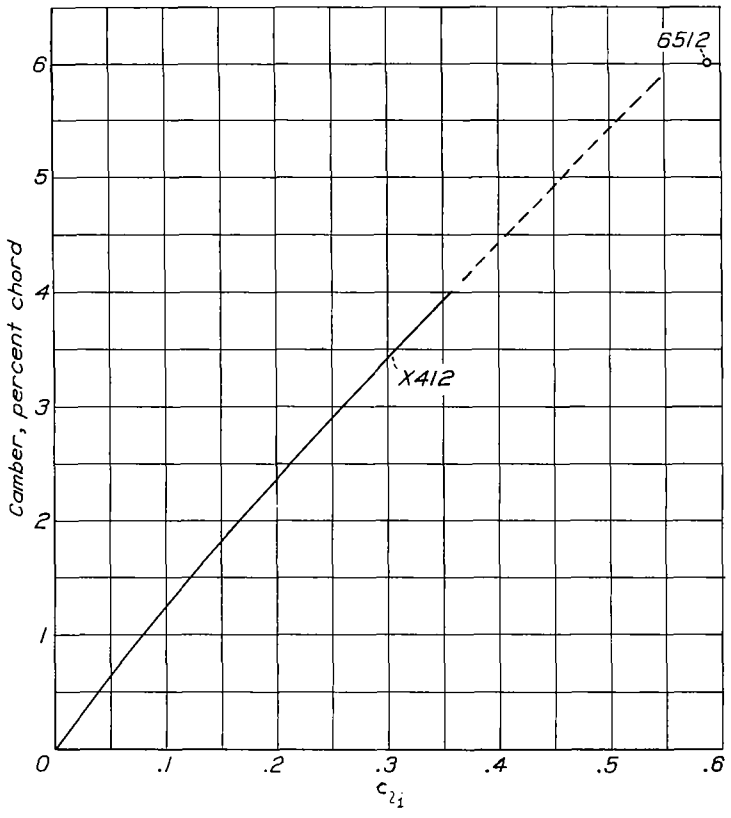

Figure 11.- Camber corresponding to the minimum peak velocity for a given lift coefficient for airfoils of the N.A.C.A. family.

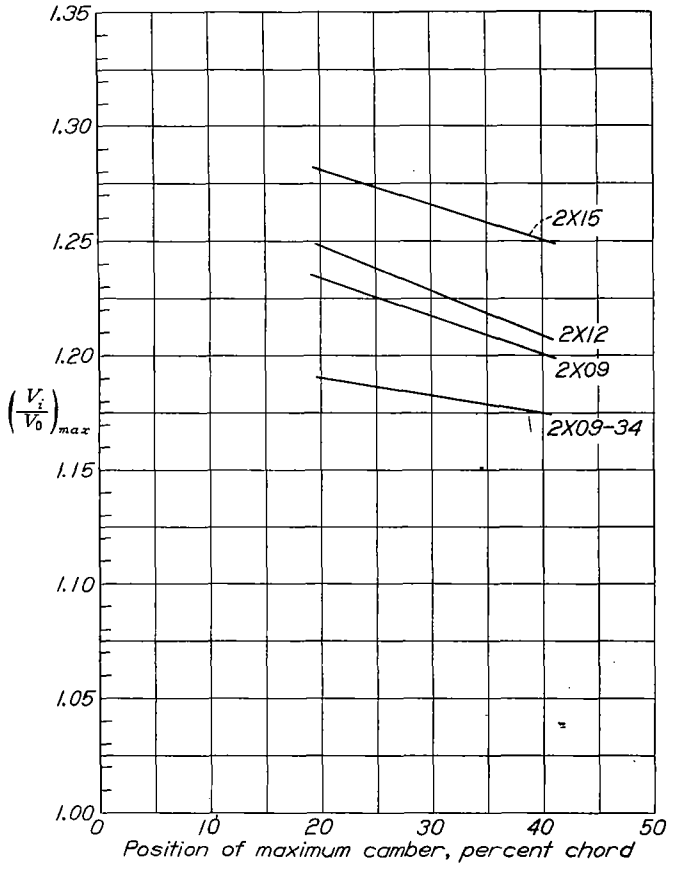

Figure 12.- Variation of peak velocities with position of maximum camber. The value of c_{ℓ_i} in each case is that for which the peak velocity is minimum. Airfoils belong to the N.A.C.A. family.

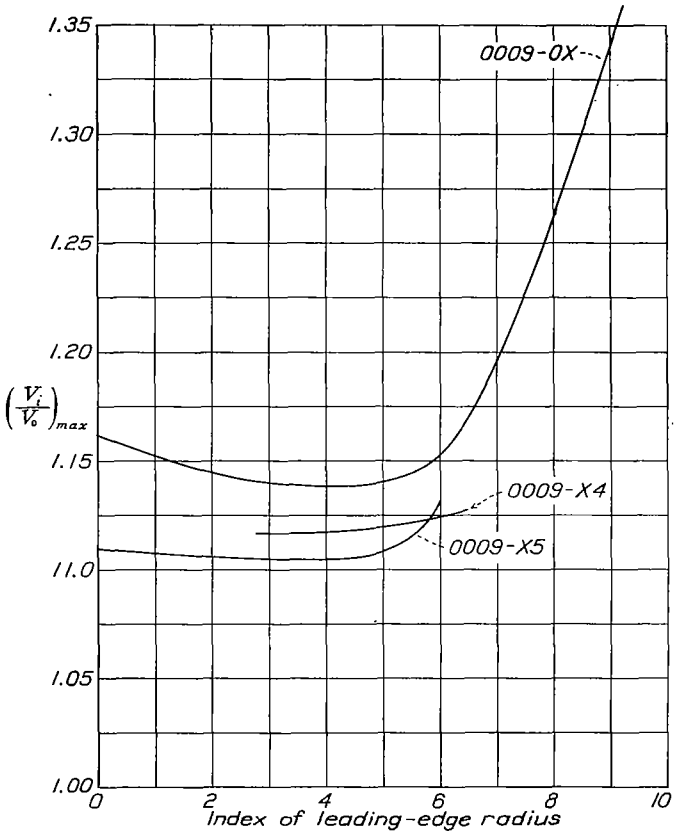

Figure 13.- Variation of peak velocities with leading-edge radius ($c_{2_i} = 0$) for airfoils of the N.A.C.A. family.